ChemComm

COMMUNICATION

View Article Online
View Journal | View Issue

Cite this: *Chem. Commun.*, 2024, **60**, 4850

Received 13th February 2024,
Accepted 31st March 2024

DOI: 10.1039/d4cc00715h

rsc.li/chemcomm

Surface modified copper foam with cobalt phthalocyanine carbon nanotube hybrids for tuning CO_2 reduction reaction products†

Javier O. Rivera-Reyes,[ab] Keith J. Billings,[c] Carmen L. Metzler,[ab] Richard M. Lagle,[d] Mebougna Drabo,[d] Ratnakar Palai,[e] John-Paul Jones[c] and Dalice M. Piñero Cruz *[ab]

The CO_2 reduction reaction (CO_2RR) is a feasible way to convert this greenhouse gas into molecules of industrial interest. Herein we present the modification of the Cu foam cathode using molecular catalyst hybrid from cobalt phthalocyanine (CoPc) to increase selectivity and stability towards CO_2RR products in a flow cell setup.

Conversion of carbon dioxide (CO_2) to useful products *via* electrochemical reduction is a promising and feasible approach to mitigate the effect resulting from anthropogenic CO_2. Moreover, the possibility to drive the CO_2 reduction reaction (CO_2RR) using renewable energy sources is of great interest in the quest to decrease CO_2 emissions. One advantage of CO_2RR is the possibility to attain a wide array of products like carbon monoxide (CO), formic acid (HCOOH), methane (CH_4) and ethylene (C_2H_4), among others.[1–3] It is important to note CO_2 is a stable molecule with a high bond dissociation energy of 532.18 kJ mol^{-1} and high activation potential of −1.90 V *vs.* SHE.[2–5] The commercial viability of CO_2RR will depend on satisfying certain parameters like high current density, high selectivity, and low overpotential. Therefore, the development and advancement of CO_2RR relies on the availability of efficient, selective, robust, and cost-effective electrocatalysts.

Among the many heterogenous electrocatalysts known, copper (Cu) is considered to have a unique capacity to produce C_{2+} products from CO_2RR. A screening study of different transition metals by Bagger *et al.*[6] reported that Cu's ability to reduce CO_2 to C_{2+} is due to a negative binding energy for CO* (ΔE_{CO*}) and a positive value for H* binding energy (ΔE_{H*}). Among the assessed metals, Cu was the only one to show this trait providing better insight into Cu's preference for producing hydrocarbons and alcohols. However, low selectivity and hydrogen evolution reaction (HER) tend to suppress Cu's ability to reduce CO_2. To address these issues and improve the selectivity of the desired C_{2+} products, approaches like doping of the Cu surface and using highly crystalline Cu materials are usually employed. Additionally, research shows doping with precious metals like Ag, Au, and Pd enhances the formation of hydrocarbons. Recent studies report on the synergistic effect of adding Au to Cu materials which promotes the formation of more difficult to attain C_{2+} products like ethanol and other high degree hydrocarbons.[7,8] Silver metal is known for efficiently converting CO_2 to CO and, when acting as a doping agent with Cu, Ag can play an active role in suppressing HER and supplying the available Cu sites with CO to form ethanol.[9] Additionally, a reported Cu–Pd electrocatalyst significantly enhanced the production of hydrocarbons based on the stoichiometry of the Cu and Pd in the electrocatalyst.[10] In fact, the researchers reported greater than 80% selectivity towards C_1 products and greater than 60% selectivity for C_{2+} when using the CuPd and Cu_3Pd electrocatalysts, respectively.[10]

The development of molecular catalysts is crucial for the optimization of the CO_2RR due to their high product selectivity and tunability. Metal phthalocyanines, the synthetic analogues of porphyrins, are an attractive catalytic material due to their low cost, durability, and excellent ability to reduce CO_2.[11–16] Phthalocyanines are a tetradentate ligand system with one available coordination site. Upon coordination of the metal centre, two additional axial coordination sites become available.[17] In particular, cobalt complexes of this family of ligands have drawn a lot of attention thanks to their high faradaic efficiency (FE) toward CO production and low cost. However, molecular catalysts are commonly tested in homogenous conditions and H-cell type reactors, which lowers stability, kinetics, and increases mass transfer

[a] *Chemistry Department, College of Natural Sciences, Rio Piedras Campus, University of Puerto Rico, San Juan, PR 00931-3346, USA. E-mail: dalice.pinero@upr.edu*
[b] *Molecular Science Research Center, University of Puerto Rico, 1390 Ponce de León, San Juan, PR 00926, USA*
[c] *Jet Propulsion Laboratory, California Institute of Technology, Pasadena, CA 91109, USA*
[d] *Department of Mechanical Engineering, Alabama A&M University, Huntsville, Alabama 35762, USA*
[e] *Department of Physics, College of Natural Sciences, Rio Piedras Campus, University of Puerto Rico, San Juan, PR, 00936, USA*

† Electronic supplementary information (ESI) available. See DOI: https://doi.org/10.1039/d4cc00715h

limitations.[18–21] The incorporation of carbon-based materials like carbon nanotubes, graphite, and carbon black with molecular catalysts leads to improved stability, retention of product selectivity, and increased conductivity of the materials.[20] The developed hybrid materials are usually tested under heterogenous conditions by immobilizing the hybrid material in a gas diffusion layer (GDL) and using techniques such as drop casting, brush, dip, and spray coating. The work by Li and colleagues focuses on the functionalization of a Cu surface with iron porphyrin causing a higher CO concentration enabling C–C coupling leading to formation of C_{2+} products like ethylene and ethanol.[22] Recently, researchers have moved towards the use of flow cells. Flow cells offer the advantages of overcoming the inherent mass transport limitations of the typical H-cells, bypassing solubility issues of CO_2 in aqueous medium by continuously supplying CO_2 at the cathode, and removing the products formed.[18,20] The flow cell design consists of a cathode where CO_2 is reduced, an anode catalyst for the oxygen evolution reaction (OER), and a polymer electrolyte membrane (PEM) between both electrodes.

The goal of the work reported here is to demonstrate the ability to regulate HER and improve CO_2RR activity on a commercially available copper foam (Cu foam) by non-covalent surface modification with cobalt phthalocyanine (CoPc) hybrid materials. The hybrid material used was a composite of CoPc with functionalized multi-walled carbon nanotubes (f-MWCNTs), as described in the ESI.† Characterization of the hybrid materials included Raman spectroscopy, powder X-ray diffraction (PXRD), X-ray photoelectron spectroscopy (XPS), scanning electron microscopy (SEM), inductively coupled plasma optical emission spectroscopy (ICP-OES), and thermogravimetric analysis (TGA). *Ex situ* Raman and SEM were performed to analyse the integrity of the electrocatalysts after CO_2 electrolysis. Systematic studies of the featured electrodes were performed at different applied full cell potentials to determine the optimal potential at which the CO_2RR could be maximized, while HER was mitigated. The grafting of the Cu foam with the bare CoPc and CoPc hybrid materials led to the reduction of H_2 FE by half (~60% to ~30%). Interestingly, the bare CoPc modification only mitigated the H_2 formation and did not affect the CO_2 product formation. In contrast, the CoPc hybrid modified Cu foam showed a ten-fold increase in CO formation. The best feature exhibited by the CoPc hybrid modified Cu foam is its high stability during extended periods of time and the rather high CO formation as time passed at 2.75 V full cell voltage and stable current density (J_{total}).

To obtain the reported hybrid material, equal amounts of in-house prepared f-MWCNTs were combined with CoPc, sonicated, and vigorously stirred overnight. The grafting of the –COOH moieties on the MWCNTs surface was confirmed in Fig. 1a *via* TGA performed at a rate of 20 °C min^{-1} under nitrogen ($N_{2(g)}$). The pristine MWCNTs exhibited only one decomposition above 600 °C attributed to carbon nanotube degradation. In contrast, the COOH functionalized MWCNTs presented three thermal decomposition zones attributed to adsorbed water, decarboxylation, and MWCNTs decomposition (Fig. S1, ESI†). The CoPc and CoPc hybrid TGA derivative weight loss and percent weight loss curves are compared in Fig. 1a and Fig. S2 (ESI†), respectively. The derivation curves in Fig. 1a of the CoPc exhibits only one thermal degradation peak with an onset around 440 °C. As expected, the hybrid material thermal degradation region has a larger area than the bare CoPc, indicating successful integration of both materials. Based on the found Co weight percent of 6.3 wt%, the CoPc weight percent on the CoPc hybrid material was found to be 60.1 wt% (Table S1, ESI†).

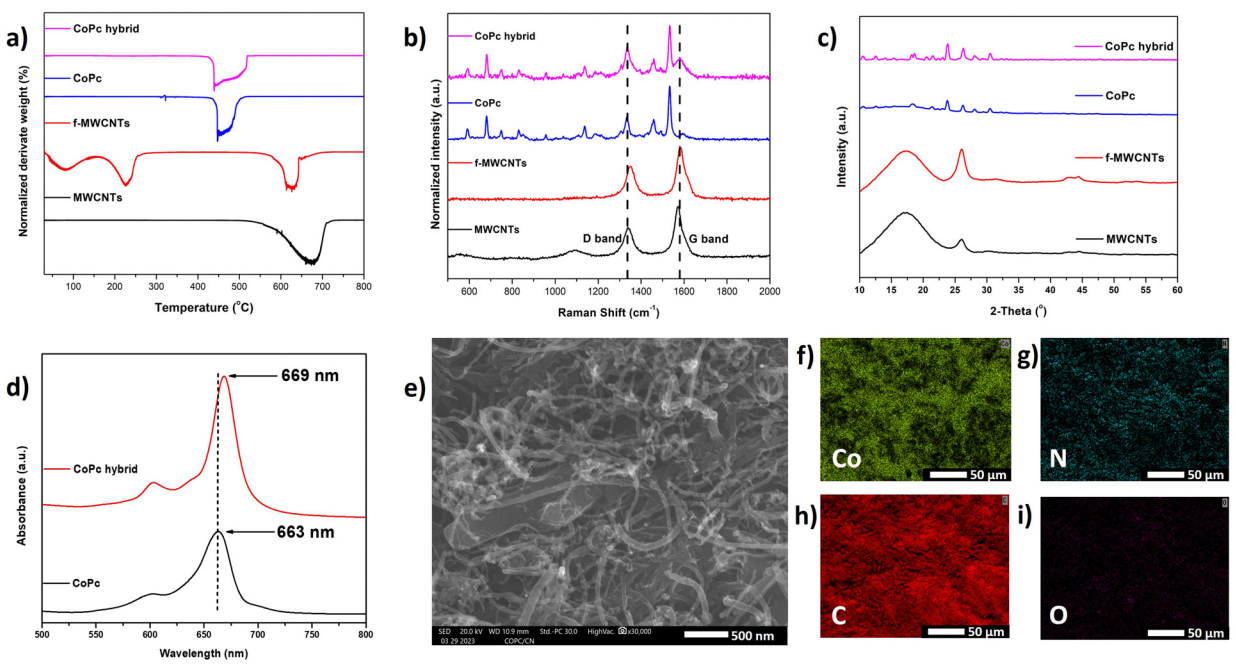

Fig. 1 Characterization of MWCNTs, f-MWCNTs, CoPc, and CoPc hybrid. (a) TGA derivative weight loss, (b) Raman spectra, (c) PXRD, (d) UV-Vis spectroscopy of CoPc and CoPc hybrid in DMF, (e) SEM image of CoPc hybrid pre-electrolysis, and (f)–(i) elemental mapping of CoPc.

Raman spectroscopy was used to further characterize the carbon nanotubes and the prepared hybrid material (Fig. 1b). The MWCNTs exhibit the characteristic D and G bands at 1338 cm^{-1} and 1572 cm^{-1}, respectively, with an I_D/I_G ratio of 0.60. The I_D/I_G ratio is used to determine the degree of disorder and defects of the MWCNTs. A higher I_D/I_G ratio indicates structural defects due to the presence of more sp^3 carbons.[23,24] The peak location of the D and G band shifted about 12 cm^{-1} and 8 cm^{-1}, respectively, after oxidative treatment. This behaviour is caused by the addition of carboxylic functional groups to the walls of the carbon nanotubes.[23,24] In addition, the f-MWCNTs I_D/I_G ratio increased to 0.64, suggesting more defects present on the surface of the carbon nanotubes. The CoPc Raman spectrum exhibits characteristic peaks at similar wavenumber values as the f-MWCNTs. The increase in intrinsic defects on the f-MWCNTs has been linked to enhanced CO_2RR catalytic activity by providing new catalytic sites.[25] After preparation of the hybrid materials the overlapping peaks intensified confirming the integration of CoPc and the f-MWCNTs. The G and D bands increased by a factor of 1.38 and 3.0, respectively, for the CoPc hybrid material in comparison to the CoPc. Additionally, PXRD was used to assess the crystallinity of the reported acid functionalized MWCNTs and hybrid material in Fig. 1c. Upon acid functionalization, the peak at 26° corresponding to the (002) hexagonal graphite plane intensified.[26] After preparation of the hybrid materials, the CoPc peaks were preserved and the (002) peak of the f-MWCNTs intensified.

Systematic XPS analysis was performed to study the chemical composition of the MWCNTs, f-MWCNTs, and the CoPc hybrid material. Fig. S3a–d (ESI†) show the MWCNTs and f-MWCNTs mainly contain C and O. The f-MWCNTs present an additional peak in the C 1s spectrum corresponding to the O–C═O bond, also the C═O band in the O 1s spectrum increases after the acidification process. In Fig. S4 (ESI†) the C, O, N, and Co XPS spectra of the CoPc hybrids demonstrate the incorporation of the CoPc to the f-MWCNTs. The observed shifts in the XPS spectra of the CoPc hybrids indicate successful combination of both materials and axial coordination of the carboxylic groups of the f-MWCNTs with the CoPc can be inferred. UV-Vis spectroscopy of the CoPc hybrid in DMF is observed in Fig. 1d. The CoPc hybrid exhibits a 6 nm bathochromic shift of its characteristic Q band. The observed shifts suggest axial coordination of the CoPc with the oxygens from the carboxylic groups on the MWCNTs.[27]

The SEM images on Fig. S5a and b (ESI†) show the MWCNTs before and after functionalization; no deformation or loss of the nanotube structure is observed. Furthermore, Fig. 1e showcases the SEM image of the CoPc hybrid exhibiting the coexistence of f-MWCNTs and CoPc. Also, elemental mapping demonstrated homogenous distribution of the CoPc elements (Co, C, N) throughout the f-MWCNTs (Fig. 1f–j).

The CO_2RR performance was examined on a zero-gap membrane reactor (Fig. S6, ESI†) using modified Cu as the cathode. The anode was also prepared in-house by spray coating IrO_2 on a platinized Ti felt (1 mg cm^{-2}). Humidified CO_2 was passed through at a rate of 100 sccm and delivered at the back of the cathode and the selected anolyte was 100 mM aqueous solution of $KHCO_3$. In between the cathode and the anode was an anionic exchange membrane (AEM) (Sustainion®). The performance of the Cu foam cathodes was surveyed over a cell voltage range of 2.5–3.25 V with 0.25 V steps.

In Fig. 2a, the CO_2RR performance of the bare Cu foam peaks at 2.75 V with a J_{total} of *ca.* 10 mA cm^{-2} (Fig. S7a, ESI†). At this voltage, it presented FE of 5.2%, 58%, 14%, and 0% for FE_{CO}, FE_{H_2}, FE_{CH_4}, and $FE_{C_2H_4}$, respectively. The bare CoPc modified Cu foam also performs optimally at 2.75 V with FE_{CO}, FE_{H_2}, and FE_{CH_4} of 4.6%, 30%, and 13%, respectively (Fig. 2b). Interestingly, the addition of CoPc resulted in a reduction of H_2 formation from 58% to 30% and a similar J_{total} output of approximately 10 mA cm^{-2} (Fig. S7b, ESI†). However, upon increasing the applied cell voltage there was a significant decrease in the CO_2RR products (Fig. 2b). Nonetheless, the CoPc hybrid modified Cu foam outperformed the previous electrodes in terms of CO_2RR product formation at the same optimal cell voltage (2.75 V), reaching FE_{CO} of 51% (Fig. 2c). Moreover, the FE_{H_2} decreased to 28%, more than half the value observed for the bare Cu foam. The suppression of HER with the modified Cu foam electrodes is attributed to higher surface area and increased CO_2 concentration ultimately favouring the CO_2RR.[22,28] Meanwhile, at 2.5 V, hydrogen is the predominant product yielding a FE_{H_2} of 50%, while the FE_{CO} is at 43%. Increasing the voltage to 3.0 V and 3.25 V hinders CO_2RR selectivity significantly as seen from Fig. 2c, while the FE_{H_2} is increased becoming the major product. In addition, at the higher voltages (3.0 V and 3.25 V) the CoPc hybrid modified Cu foam produced C_2H_4 in small quantities, *ca.* 3%. Long-term study of the CoPc hybrid modified Cu foam performance at 2.75 V present attenuation of the J_{total} over the course of 18 hours (Fig. S8a, ESI†).[27] Although, there is a decrease in J_{total} (Fig. S8b, ESI†), the CO selectivity is not compromised and increases as time passes as shown in Fig. S8a (ESI†). Overall, the modification of the Cu foam with the bare CoPc and CoPc hybrid reduces by half the H_2 production compared to the bare Cu foam. Also, the full cell energy efficiency ($EE_{full\ cell}$) was determined for each of the quantified products (CO, CH_4, C_2H_4) as depicted in Fig. S9 (ESI†). The CoPc hybrid modified Cu foam presented the highest $EE_{full\ cell}$ for CO and C_2H_4 with values of 25% and 3%, respectively.

After the electrolysis experiments, the CoPc hybrid modified Cu foam and the AEM were retrieved and analysed with Raman spectroscopy, and SEM. In Fig. 3, the Raman spectra of the CoPc and f-MWCNTs confirm no degradation of the materials after extended periods of electrolysis (~18 hours). Moreover, all characteristic peaks associated with the f-MWCNTs and CoPc are present and in accordance with the hybrid material before electrolysis. An additional SEM image after electrolysis of the CoPc hybrid material exhibited the presence of intact MWCNTs structure (Fig. S10, ESI†).

To summarize, we have successfully developed a non-covalent surface modification of Cu foam using a molecular catalyst hybrid. This modification strategy served to regulate HER and increase selectivity towards CO_2RR products. Furthermore, characterization of the axially coordinated hybrid materials before and after the electrolytic experiments ensured the

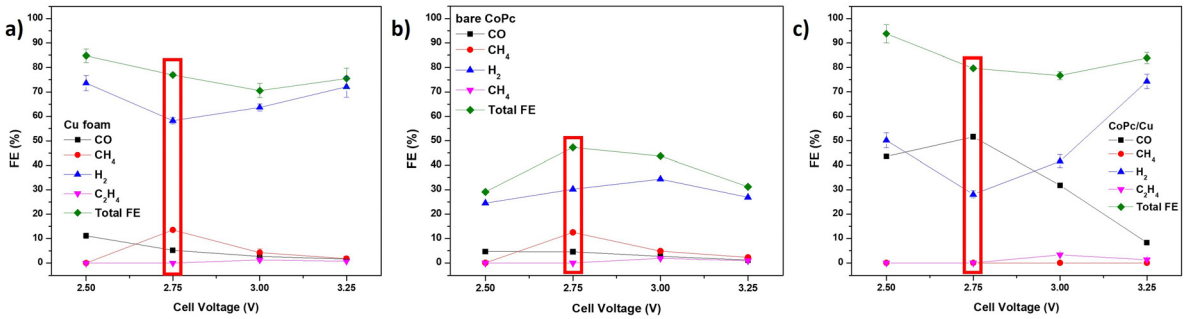

Fig. 2 Faradaic efficiencies at different full cell voltages (a) bare Cu foam, (b) CoPc modified Cu foam, and (c) CoPc hybrid modified Cu foam (red enclosure denotes optimal voltage).

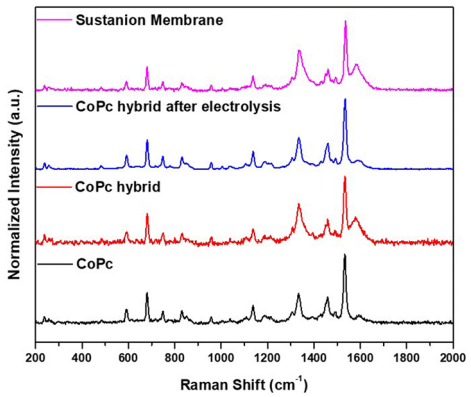

Fig. 3 Raman spectra of CoPc hybrid after electrolysis.

stability of the tested materials. The bare CoPc and CoPc hybrid exhibited an optimal voltage of 2.75 V resulting in a substantial decrease in the FE_{H_2} of *ca.* 60% to *ca.* 30%. In the case of the CoPc hybrid, the CO formation increased ten-fold when compared to the bare Cu foam and bare CoPc. Importantly, the CoPc hybrid material exhibited long-term stability for an electrolysis period of 18-hour. The work presented herein provides a straightforward methodology to enhance the CO_2RR performance, while offering valuable insight into the modulation of CO_2RR selectivity in Cu foam *via* non-covalent interactions.

This research was funded by PR Space Grant Consortium and NASA Cooperative Agreement grant number 80NSSC20M0052. Part of the research was carried out at the Jet Propulsion Laboratory, California Institute of Technology, under a contract with the National Aeronautics and Space Administration (80NM0018D0004). C. L. M. acknowledges the support from NIH RISE Grant number 5R25GM061151-22.

Conflicts of interest

There are no conflicts to declare.

Notes and references

1 R. Francke, B. Schille and M. Roemelt, *Chem. Rev.*, 2018, **118**, 4631–4701.
2 W. Zhang, Y. Hu, L. Ma, G. Zhu, Y. Wang, X. Xue, R. Chen, S. Yang and Z. Jin, *Adv. Sci.*, 2018, **5**, 1700275.
3 M. Jitaru, *J. Chem. Technol. Metall.*, 2007, **42**, 333–344.
4 B. Ruscic, D. Feller and K. A. Peterson, *Theor. Chem. Acc.*, 2014, **133**, 1415.
5 C. Jiang, A. W. Nichols and C. W. Machan, *Dalton Trans.*, 2019, **48**, 9454–9468.
6 A. Bagger, W. Ju, A. S. Varela, P. Strasser and J. Rossmeisl, *ChemPhysChem*, 2017, **18**, 3266–3273.
7 C. G. Morales-Guio, E. R. Cave, S. A. Nitopi, J. T. Feaster, L. Wang, K. P. Kuhl, A. Jackson, N. C. Johnson, D. N. Abram, T. Hatsukade, C. Hahn and T. F. Jaramillo, *Nat. Catal.*, 2018, **1**, 764–771.
8 D. Kim, J. Resasco, Y. Yu, A. M. Asiri and P. Yang, *Nat. Commun.*, 2014, **5**, 4948.
9 S. Lee, G. Park and J. Lee, *ACS Catal.*, 2017, **7**, 8594–8604.
10 S. Ma, M. Sadakiyo, M. Heima, R. Luo, R. T. Haasch, J. I. Gold, M. Yamauchi and P. J. A. Kenis, *J. Am. Chem. Soc.*, 2017, **139**, 47–50.
11 M. Zhu, J. Chen, L. Huang, R. Ye, J. Xu and Y. Han, *Angew. Chem., Int. Ed.*, 2019, **58**, 6595–6599.
12 T. Yoshida, K. Kamato, M. Tsukamoto, T. Iida, D. Schlettwein, D. Wöhrle and M. Kaneko, *J. Electroanal. Chem.*, 1995, **385**, 209–225.
13 X. Zhang, Z. Wu, X. Zhang, L. Li, Y. Li, H. Xu, X. Li, X. Yu, Z. Zhang, Y. Liang and H. Wang, *Nat. Commun.*, 2017, **8**, 14675.
14 X. Chen, X. M. Hu, K. Daasbjerg and M. S. G. Ahlquist, *Organometallics*, 2020, **39**, 1634–1641.
15 X.-M. Hu, M. H. Rønne, S. U. Pedersen, T. Skrydstrup and K. Daasbjerg, *Angew. Chem., Int. Ed.*, 2017, **56**, 6468–6472.
16 H. Tanaka and A. Aramata, *J. Electroanal. Chem.*, 1997, **437**, 29–35.
17 A. B. Sorokin, *Chem. Rev.*, 2013, **113**, 8152–8191.
18 D. M. Weekes, D. A. Salvatore, A. Reyes, A. Huang and C. P. Berlinguette, *Acc. Chem. Res.*, 2018, **51**, 910–918.
19 D. Salvatore and C. P. Berlinguette, *ACS Energy Lett.*, 2020, **5**, 215–220.
20 S. Ren, D. Joulié, D. A. Salvatore, K. Torbensen, M. Wang, M. Robert and C. P. Berlinguette, *Science*, 2019, **365**, 367–369.
21 D. A. Salvatore, D. M. Weekes, J. He, K. E. Dettelbach, Y. C. Li, T. E. Mallouk and C. P. Berlinguette, *ACS Energy Lett.*, 2018, **3**, 149–154.
22 F. Li, Y. C. Li, Z. Wang, J. Li, D.-H. Nam, Y. Lum, M. Luo, X. Wang, A. Ozden, S.-F. Hung, B. Chen, Y. Wang, J. Wicks, Y. Xu, Y. Li, C. M. Gabardo, C.-T. Dinh, Y. Wang, T.-T. Zhuang, D. Sinton and E. H. Sargent, *Nat. Catal.*, 2019, **3**, 75–82.
23 L. Thi Mai Hoa, *Diamond Relat. Mater.*, 2018, **89**, 43–51.
24 B. Scheibe, E. Borowiak-Palen and R. J. Kalenczuk, *Mater. Charact.*, 2010, **61**, 185–191.
25 W. Wang, L. Shang, G. Chang, C. Yan, R. Shi, Y. Zhao, G. I. N. Waterhouse, D. Yang and T. Zhang, *Adv. Mater.*, 2019, **31**, 1808276.
26 L. N. Ramavathu, K. K. Maniam, K. Gopalram and R. Chetty, *J. Appl. Electrochem.*, 2012, **42**, 945–951.
27 H. Li, Y. Pan, Z. Wang, Y. Yu, J. Xiong, H. Du, J. Lai, L. Wang and S. Feng, *Nano Res.*, 2022, **15**, 3056–3064.
28 A. Mustafa, B. G. Lougou, Y. Shuai, Z. Wang, H. U. Rehman, S. Razzaq, W. Wang, R. Pan and J. Zhao, *Front. Chem. Sci. Eng.*, 2024, **18**, 29.